Contactless Characterization of a CMOS Integrated LC Resonator for Wireless Power Transferring

Fabian L. Cabrera, *Member, IEEE,* and F. Rangel de Sousa, *Senior Member, IEEE*

***Abstract*—Miniaturized implanted circuits must be autonomous, harvesting energy from surroundings or receiving power from an inductive link. Considering the latter, when the implant dimensions are limited to few mm^2, the power receiver must be carefully designed so that its efficiency is maximized. If the receiving inductor is integrated in a silicon substrate, a rigorous design methodology should be adopted, because the losses are high, thus degrading the power transmission efficiency. An additional issue arises when such a system needs to be tested, which must happen without invasive techniques. In this article, we describe the contactless characterization of an LC resonator used in an $1.5\ mm \times 1.5\ mm$ fully integrated wireless power receiver. A quality factor of 20.8 was measured at the resonance frequency $0.99\ GHz$.**

***Index Terms*—Contactless measurement, inductive link, integrated resonator, seal ring, wireless power transfer.**

I. Introduction

INDUCTIVE links have been extensively employed for wireless power transfer (WPT) to implanted medical devices (IMDs) [1], [2], to radio-frequency identification (RFID) tags [3], to lab-on-chip applications [2] and to bondpadless chips [4], [5], among others. The energy transfer is accomplished by means of magnetic coupling between two inductors. Most of the applications, specially the IMDs, require miniaturization of the secondary inductor to reduce the size of the systems [6]. As a consequence, the monolithic implementation in a CMOS standard process becomes a natural choice, because it may potentially reduce the costs, allow integration with the analog and digital circuitry and increase reliability. However, the quality factor of CMOS-integrated inductors is low, strongly affecting the WPT efficiency (η), which depends on the electromagnetic coupling level of the link (A) and on the load impedance matching condition (p) as can be verified by the reciprocal of the efficiency calculated by [7]:

$$\frac{1}{\eta} = \frac{1}{A}\left(p + 2 + \frac{1}{p}\right) + p + 1. \tag{1}$$

In (1), $A = k^2 Q_1 Q_2$, where k is the magnetic coupling factor and Q_1 and Q_2 are the quality factor of the external and integrated inductors, respectively. Because A must be maximized for highest efficiency and considering an integrated implanted device, it is important to investigate how to maximize the quality factor of CMOS-integrated inductors.

Manuscript received December 26, 2014; revised February 22, 2015; accepted April 10, 2015. This work was supported in part by CNPq, NAMITEC and CAPES.

The authors are with Radiofrequency Laboratory, Electrical Engineering Department, Federal University of Santa Catarina, Florianópolis, SC 88040900 Brazil. (e-mail: fabian.l.c@ieee.org, rangel@ieee.org).

Color versions of one or more of the figures in this letter are available online at http://ieeexplore.ieee.org.

Digital Object Identifier

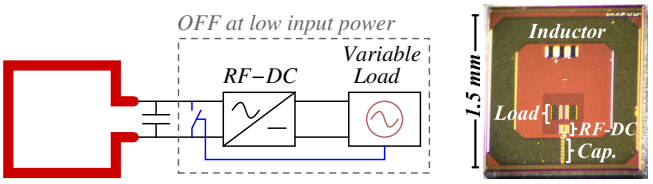

(a) Block diagram. (b) Photograph.

Fig. 1. Fully integrated wireless power receiver including the LC resonator.

Unlike general purpose inductors, the WPT inductors must occupy the outermost area of the chip to maximize the enclosed magnetic flux, and k as consequence. Therefore, the circuits must be laid out inside the inductor, which increases the complexity of the electromagnetic simulations and prevents the use of loss-reduction techniques such as substrate shielding. Furthermore, the guard rings used to isolate the standard inductors from other structures must be avoided in WPT inductors, as their interaction degrades the energy transfer efficiency. In addition to a careful design, the characterization of integrated inductors for WPT is challenging. Commonly, it is performed using microprobes to connect the device under test (DUT) to an impedance analyzer. This method requires the fabrication of dedicated structures to de-embed the electrical effects added by the test setup, which do not take into account the mutual coupling between the inductor, the pads and the probes. An alternative approach is to characterize the resonator instead of the inductor alone. In a WPT receiver, the LC resonator is formed by the interaction between the inductor and the capacitive matching network.

In this article, we present measurement results obtained from an LC resonator integrated in a $180\ nm$ CMOS technology, carefully designed to maximize the efficiency of the WPT receiver constrained in an area of $2.25\ mm^2$. We developed a contactless methodology to characterize the resonator, using a well-modeled magnetic interaction between DUT and the test setup. The two principal resonator parameters, the quality factor and the resonance frequency were measured.

II. Design and Measurement Methodology

The integrated resonator is composed of a custom-designed inductor in parallel with matching and parasitic capacitors as illustrated in Fig. 1(a). The dimensions of the inductor were optimally chosen to obtain the highest quality factor considering the technology constraints and the area restricted to

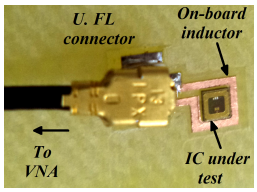

(a) Characterization setup.

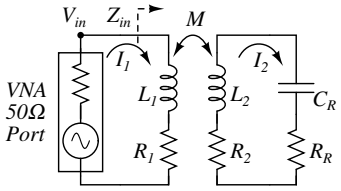

(b) Electrical model.

Fig. 2. Resonator characterization setup and model.

$1.5\ mm \times 1.5\ mm$ [8]. Full wave electromagnetic simulations using the software EMPRO® from Keysight® showed that the best inductor should have one turn, with a linewidth of $250\ \mu m$ and average diameter of $1210\ \mu m$. It was implemented in the uppermost metal level of an $180\ nm$ CMOS technology and its photograph is shown in Fig. 1(b). Moreover, the design procedure included the frequency as an optimization variable and its best value was $1.04\ GHz$, which resulted in a quality factor of 22. A dual MIM capacitor of $11.6\ pF$ was integrated to resonate with the inductor at the optimum frequency. The combination of the inductor and capacitor losses leads to a resonator quality factor of 21.7.

Several considerations were taken into account during the layout elaboration. Guard rings, large area capacitors, and high-count number of pads were avoided to reduce the effects of induced currents loops. Moreover, the power distribution tree was carefully designed for minimizing the interference on the magnetic flux.

The main characteristics of the resonator can be measured using the setup shown in Fig. 2(a). An inductor (L_1) printed on a FR4 board was used as an interface between the integrated resonator and a R&S® ZVB8 vector network analyzer (VNA). The resulting inductive link can be modeled with the circuit of Fig. 2(b). Each inductor $L_{1(2)}$ has a series equivalent resistance $R_{1(2)}$ modeling the losses. $M{=}k\sqrt{L_1 L_2}$ is the mutual inductance. C_R represents the parasitic and integrated capacitances and R_R models their losses.

According to the model of Fig. 2(b), the input impedance (Z_{in}) can be defined as:

$$Z_{in} = j\omega L_1 + R_1 + \Delta Z; \tag{2}$$

where $\Delta Z = \Delta R + j\Delta X$ accounts for the reflexion of the secondary impedance on the primary side. For convenience, the real and imaginary parts of ΔZ are normalized by the frequency as following:

$$e(\omega) = \frac{\Delta R}{\omega} = \frac{k^2 L_1 (1/Q_R)}{1/Q_R^2 + (1-\omega_0^2/\omega^2)^2} \tag{3}$$

$$g(\omega) = \frac{\Delta X}{\omega} = \frac{-k^2 L_1 (1-\omega_0^2/\omega^2)}{1/Q_R^2 + (1-\omega_0^2/\omega^2)^2}; \tag{4}$$

where $Q_R{=}\omega L_2/(R_2{+}R_R)$ is the resonator quality factor, and $\omega_0{=}1/\sqrt{L_2 C_R}$ is the resonance angular frequency. The maximum value of (3) occurs at the resonance frequency, where $e(\omega_0) = k^2 L_1 Q_R$. On the other hand, (4) has two peaks of opposite signs, that occur at the frequencies ω_{p1} and ω_{p2}:

$$\omega_{p1(2)} = \frac{\omega_0}{\sqrt{1 \pm 1/Q_R}}. \tag{5}$$

The values of $g(\omega)$ at frequencies ω_{p1} and ω_{p2} are:

$$g(\omega_{p1(2)}) = \pm\frac{k^2 L_1 Q_R}{2}. \tag{6}$$

Using (5), we determine the value Q_R from the ratio between ω_{p1} and ω_{p2} as following:

$$Q_R = \frac{1 + (\omega_{p1}/\omega_{p2})^2}{1 - (\omega_{p1}/\omega_{p2})^2}. \tag{7}$$

From the development above, we can devise a method for the contactless characterization of the integrated resonator as following:

1) Using the setup of Fig. 2(a), Z_{in} is measured in a range of frequencies around the expected resonance frequency, spanning beyond ω_{p1} and ω_{p2}. The measurement of Z_{in} is performed in the presence (Z_w) and in the absence (Z_{wo}) of the resonator.
2) The curve $e(\omega)$ is obtained from $\Re\{Z_w{-}Z_{wo}\}/\omega$.
3) The value of ω_0 is determined from the observation of the frequency where the maximum of $e(\omega)$ occurs.
4) Inductance L_1 is found by $\Im\{Z_w(\omega_0)\}/\omega_0$.
5) Detecting the frequencies where the maximum and the minimum of $\Im\{Z_w{-}j\omega L_1\}/\omega$ occur and using (7), we determine Q_R.
6) By calculating the peak-to-peak value (g_{pp}) of $\Im\{Z_w{-}j\omega L_1\}/\omega$ and using (6), the magnetic coupling factor k is found from:

$$k = \sqrt{\frac{g_{pp}}{L_1 Q_R}}. \tag{8}$$

III. Results and Discussion

The printed inductor used to measure the resonator characteristics has an average diameter of $2.4\ mm$ and linewidth $0.6\ mm$. These dimensions were chosen to be as close as possible to the size of the chip, ensuring that $k^2 Q_1 Q_2$ is high enough. The power of the source signal was $-10\ dBm$, which is sufficiently low not to turn-on the active circuitry connected to the resonator (Fig. 1(a)).

The measured values of $e(\omega)$ and $g(\omega)$ are compared with the simulations in Fig. 3. Two cases were considered: a) first we measured the chip surrounded by a crack-stop (CS) ring (also known as seal ring), which is a structure inserted by the manufacturer for protecting the die during dicing and packaging [9]; b) then, we measured the chip after breaking the CS ring (opening it). Both simulations and measurements showed that the closed CS ring diminishes the quality factor and shifts the resonance frequency to a higher value, reflecting a reduction on the value of L_2. These effects are caused by the currents induced in the closed CS ring.

The measurement method described in the previous section was applied to 38 samples of the chip surrounded by the closed CS ring and to 5 samples with the CS ring open. The results are summarized in table I . The measured quality factor is very near to the predicted values in both cases tested. However, the resonant frequency measured is about $50\ MHz$ lower than simulations in both cases, which corresponds to a prediction error of approximately 5%. The difference can be attributed to

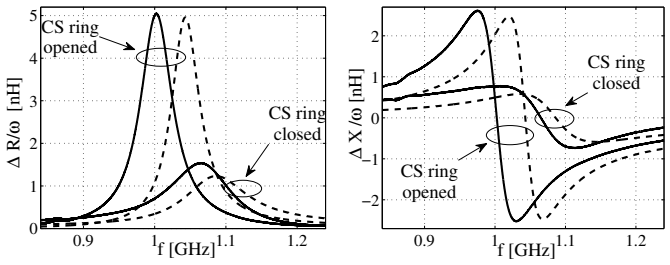

(a) Normalized resistance. (b) Normalized reactance.

Fig. 3. Impedance variation measured (solid line) and simulated (dashed line).

TABLE I
MEAN AND STANDARD DEVIATION (SD) OF THE INTEGRATED RESONATOR CHARACTERISTICS.

	CS ring closed			CS ring opened		
	Simulated	Measured		Simulated	Measured	
		Mean	SD		Mean	SD
f_0 [GHz]	1.12	1.07	0.003	1.04	0.99	0.005
L_1 [nH]	3.31	2.67	0.009	3.51	2.96	0.03
Q_R	10.5	11.0	0.3	21.7	20.8	0.6
k	0.18	0.23	0.002	0.26	0.31	0.002

inaccuracy in the calculation of the parasitic capacitances and to the effects of the circuits laid out inside the inductor, which are difficult to include in the electromagnetic simulations. The quality factor is also plotted in Fig. 4, where the dispersion of the measurement can be observed.

Table II compares the results obtained in this work with other miniaturized inductors for WPT. Only the references [2], [4], [5] and this work have integrated inductors in conventional CMOS technologies without post-processing. In that group our inductor achieved the best quality factor, noting that newer technologies have some additional advantages. For example, the $180\ nm$ CMOS process used in this work has one top thick metal layer, while some $130\ nm$ and newer CMOS processes have two or more thick metal layers, which can potentially increase the quality factor of inductors.

IV. CONCLUSION

In this paper we presented a contactless method for measuring the resonance frequency and the quality factor of an integrated resonator . The method is based on the observation of the input impedance of a strongly coupled inductive link. The method was applied to characterize an LC resonator integrated in a $180\ nm$ standard CMOS process occupying

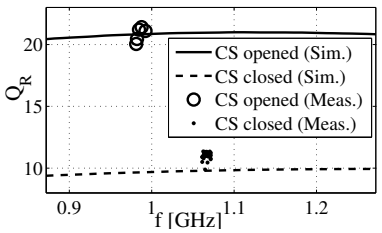

Fig. 4. Quality factor of the integrated resonator.

TABLE II
MINIATURIZED INDUCTORS FOR WIRELESS POWER TRANSFERRING.

	Area [mm²]	Technology	Q	f [MHz]	Test method
[4]	6.25	CMOS 350 nm	2.6	900	–
[3]	0.5	CMOS 130 nm post-processing	3	2450	Wired
[2]	4.84	CMOS 130 nm	11	101	Wired microprobe
[5]	0.5	CMOS 130 nm	14	5200	Wired
[6]	20.25	High-resistivity substrate and post-processing	20	2.5	Wired microprobe
This work	2.25	CMOS 180 nm	20.8	990	Contactless
[10]	4.96	SU-8-based MEMS	29	394	–

an area of $1.5\ mm \times 1.5\ mm$. Two cases were considered: a) The circuit involved by a crack-stop ring; b) The crack-stop ring was broken. In the case a) the quality factor measured was 11 at the resonance frequency of $1.07\ GHz$ and for the case b) the quality factor measured was 20.8 at the resonance frequency of $0.99\ GHz$. Both results confirmed the predictions from full-wave EM simulations.

In terms of the experimental verification of the miniaturized inductors, it is important to note the advantages of using a contactless method. The integrated resonator can be tested without modifying the application circuit. On the other hand, wired methods often imply the fabrication of the inductor separated from the other circuits or modification of the on-chip connections by using laser [5].

REFERENCES

[1] M. Nazari, M. Mujeeb-U-Rahman, and A. Scherer, "An implantable continuous glucose monitoring microsystem in 0.18 μm CMOS," in *Dig. Tech. Pap. Symp. VLSI Circuits*, Jun. 2014, pp. 1–2.

[2] M. Zargham and P. Gulak, "Fully integrated on-chip coil in 0.13 μm CMOS for wireless power transfer through biological media," *IEEE Trans. Biomed. Circuits Syst.*, vol. PP, no. 99, pp. 1–1, 2014.

[3] X. Chen, W.-G. Yeoh, Y. B. Choi, H. Li, and R. Singh, "A 2.45-GHz near-field RFID system with passive on-chip antenna tags," *IEEE Trans. Microw. Theory Tech.*, vol. 56, no. 6, pp. 1397–1404, Jun. 2008.

[4] S. Luan, A. Eftekhar, O. Murphy, and T. Constandinou, "Towards an inductively coupled power/data link for bondpad-less silicon chips," in *Proc. IEEE Int. Symp. Circuits Syst.*, May 2011, pp. 2597–2600.

[5] A. Shamim, M. Arsalan, L. Roy, M. Shams, and G. Tarr, "Wireless dosimeter: System-on-chip versus system-in-package for biomedical and space applications," *IEEE Trans. Circuits Syst. II*, vol. 55, no. 7, pp. 643–647, July 2008.

[6] R. Wu, S. Raju, M. Chan, J. Sin, and C. Yue, "Silicon-embedded receiving coil for high-efficiency wireless power transfer to implantable biomedical ICs," *IEEE Electron Device Lett.*, vol. 34, no. 1, pp. 9–11, Jan. 2013.

[7] F. L. Cabrera and F. R. d. Sousa, "Optimal design of energy efficient inductive links for powering implanted devices," in *Proc. IEEE Topical Conf. Biomedical Wireless Technol., Networks and Sensing Syst.*, Jan. 2014, pp. 1–3.

[8] F. L. Cabrera and F. R. d. Sousa, "A CMOS fully-integrated wireless power receiver for autonomous implanted devices," in *Proc. IEEE Int. Symp. Circuits Syst.*, Jun. 2014, pp. 1–4.

[9] S.-H. Chen and M.-D. Ker, "Investigation on seal-ring rules for IC product reliability in 0.25-μm CMOS technology," *Microelectronics Reliability*, vol. 45, no. 911, pp. 1311 – 1316, 2005.

[10] S.-H. Cho, N. Xue, L. Cauller, W. Rosellini, and J.-B. Lee, "A SU-8-based fully integrated biocompatible inductively powered wireless neurostimulator," *J. Microelectromech. Syst.*, vol. 22, no. 1, pp. 170–176, Feb. 2013.